Geochemistry Geophysics Geosystems G3

Article
Volume 11
11 May 2010
Q0AC02, doi:10.1029/2009GC002798
ISSN: 1525-2027

Published by AGU and the Geochemical Society

Isotopic evidence for chaotic imprint in upper mantle heterogeneity

Pietro Armienti
Dipartimento di Scienze della Terra, Università di Pisa, via S. Maria, I-56126 Pisa, Italy (armienti@dst.unipi.it)

Daniela Gasperini
Departamento de Geoquímica, Petrologia i Prospecció Geològica, Universitat de Barcelona, E-08028 Barcelona, Spain

[1] The intrinsic structure of the isotope data set of samples from the Mid-Atlantic Ridge and East Pacific Rise, believed to represent the isotopic composition of their mantle source, reveals a close relationship between sample spatial distribution and their geochemical features. The spatial distribution of their isotopic heterogeneity is self-similar on a scale between 5000 and 6000 km (about 1/6 of Earth's circumference), suggesting a self-organized structure for the underlying mantle. This implies the imprint of chaotic mantle processes, induced by mantle flow and likely related to an early phase of highly dynamic behavior of the Earth's mantle. The size of the identified self-organized region reflects the large length scale of upper mantle chemical variability, and it is likely frozen since the Proterozoic. The geochemical heterogeneity of the asthenosphere along the ridges is believed to record a transition in the thermal conditions of the Earth's mantle and to be reflected in the $l = 6$ peak expansion of several geophysical observables.

Components: 11,300 words, 5 figures, 1 table.

Keywords: MORB; asthenosphere; chaotic dynamics; isotope geochemistry; mantle convection.

Index Terms: 8125 Tectonophysics: Evolution of the Earth (0325); 4485 Nonlinear Geophysics: Self-organization.

Received 24 August 2009; **Revised** 4 February 2010; **Accepted** 3 March 2010; **Published** 11 May 2010.

Armienti, P., and D. Gasperini (2010), Isotopic evidence for chaotic imprint in upper mantle heterogeneity, *Geochem. Geophys. Geosyst.*, *11*, Q0AC02, doi:10.1029/2009GC002798.

Theme: Geochemical Heterogeneities in Oceanic Island Basalt and Mid-ocean Ridge Basalt Sources: Implications for Melting Processes and Mantle Dynamics
Guest Editors: C. Beier and P. Asimow

1. Introduction

[2] Thanks to great improvements in analytical techniques on radioactive and stable isotope systems, the geochemistry of Mid-Ocean Ridge Basalts (MORB) is now greatly detailed. Once believed to sample a degassed (low ^{3}He, ^{40}Ar), incompatible element-poor, shallow and homogeneous mantle reservoir, MORB are now used to constrain the length scale of mantle heterogeneity, spanning from extremely long (e.g., Dupal anomaly) to very short (e.g., olivine melt inclusion) wavelengths. MORB are almost perfect for this goal since they tap the asthenosphere extensively and almost continuously

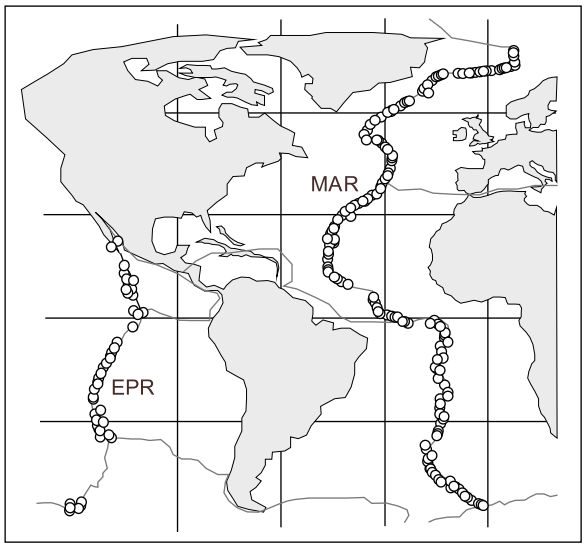

Figure 1. Sample locations (triangular symbols) along the Mid-Atlantic Ridge and East Pacific Rise. Isotope data are from PetDB (http://www.petdb.org/) and GeoROC (http://georoc.mpch-mainz.gwdg.de/Start.asp) databases and from *Agranier et al.* [2005].

and, at ridge crests, they are young and not contaminated (e.g., by seawater). To a first approximation, MORB represent partial melts of shallow mantle sources that experienced large melting degrees under geodynamic conditions which are relatively well constrained (e.g., Mid-Atlantic Ridge). The availability of large databases (e.g., Lamont PetDB and GeoROC) and new high-precision isotope data [e.g., *Agranier et al.*, 2005; *Meyzen et al.*, 2007] allowed for integration of MORB geochemical variability with latitude along ridges, the geoid and/or seismic velocity anomalies [e.g., *Klein and Langmuir*, 1987; *Cazenave et al.*, 1992; *Butler et al.*, 1993; *Humler et al.*, 1993; *Wessel et al.*, 1994, 1996; *Zhang et al.*, 1994; *Lecroart et al.*, 1997; *Goslin et al.*, 1998; *Graham et al.*, 2001; *Kellogg et al.*, 2002; *Meibom and Anderson*, 2004; *Moore et al.*, 2004; *Agranier et al.*, 2005; *Anderson*, 2006]. MORB sampled at mid-ocean ridges allows us to infer heterogeneities in the asthenospheric mantle as the ultimate effect of complex processes dominated by temperature, pressure and composition of the shallow mantle. This occurs in a convective regime that involves mass transfer from the deep mantle, occasionally disturbed by the occurrence of hot spots [e.g., *Butler et al.*, 1993; *Phipps Morgan and Morgan*, 1999; *Hofmann*, 1997; *Lecroart et al.*, 1997; *Goslin et al.*, 1998; *Saal et al.*, 1998; *Graham et al.*, 2001; *Kellogg et al.*, 2002; *Agranier et al.*, 2005; *Blichert-Toft et al.*, 2005; *Debaille et al.*, 2006]. Alternatively, upper mantle heterogeneity has been interpreted as the natural result of basically athermal processes that are intrinsic to plate tectonics, such as recycling and delamination of continental crust and subducted aseismic ridges [*Meibom and Anderson*, 2004; *Anderson*, 2006].

[3] In this paper we analyze the correlations between the isotopic (Sr, Nd, Hf, Pb) composition of MORB along both the Mid-Atlantic Ridge (MAR) and the East Pacific Rise (EPR) as a function of their position along the ridge (Figure 1). We discuss whether the theory of chaotic dynamical systems applied to isotopic series along oceanic ridges can delimit the length scale of upper mantle heterogeneities, and thus test whether the mantle structure is consistent with a self similar distribution of such heterogeneity. We recognize the topological features of the shallow mantle through the geochemical signature it sends to the surface by means of ridge basalts. This is obtained by recognizing the isomorphism (= same form) existing between a spatial structure and the geochemical signal it can supply, and that can be detected by suitable analysis of data sets.

2. Methods

2.1. Self-Similarity

[4] Self-similarity is defined by the scale-invariant relation: $n(L) = L^{-D}$, or in logarithmic form $\ln[n(L)] = -D \cdot \ln(L)$, in which it is stated that the number n of objects that composes a set of measurements depends exponentially on the size L of the "ruler" (unit of measurements or magnification) used for the data analysis, where D is a fractional value related to the Euclidean dimension of the space in which the measurement is performed. This means that if we are dealing with measurements on a line, D is a number between 0 and 1, as well as if we are dealing with "volume" measurements, D is between 2 and 3. The scale invariance relation states that the number of objects observed at different scales depends on the scale itself. In fact, if the ruler decreases in size from L to $(L - \Delta L)$ (or magnification rises), the number of measurements grows according to

$$n(L - \Delta L) = n(L)\left(\frac{L - \Delta L}{L}\right)^{-D}.$$

[5] Additional iteration of this procedure gives a multiplicative cascade that generates an infinite sequence of measures. This is a kind of regularity that fixes the aspect of the observed set indepen-

dently of the magnification of observation. Self-similarity is a typical feature of fractal sets.

2.2. Fractals and Fractal Dimension

[6] Eddies, boundary of clouds, and coastlines may be represented by curves whose common features are irregularity and nondifferentiability, that is they exhibit self-similar fluctuations. Such irregular fluctuations may be visualized to result from the superimposition of an ensemble of eddies or sine waves. Mathematical models for simulation and prediction of dynamical systems are nonlinear so that analytical solutions are not available. Finite precision computed solutions are sensitively dependent on initial conditions and give chaotic solutions, identified as deterministic chaos. A "fractal" is a set of points whose dimension exceeds its topological (Euclidean) dimension (D_E) or, using *Mandelbrot*'s [1982, p. 15] definition, "a rough or fragmented geometric shape that can be subdivided in parts, each of which is (at least approximately) a reduced/size copy of the whole." We take the ratio $D_F = -\ln[n(L)]/\ln(L)$ as the definition of "fractal dimension" of a self-similar object. In a rough sense, fractal dimension is a measure of how "complicated" a self-similar figure is or, mathematically speaking, D_F represents the degree of self-similarity. The fractal nature of a time or space series may be revealed by means of suitable mathematical techniques. The principle is that a one-dimensional time, or space, series can be expanded into a higher-dimensional space, in which the dynamic of the underlying generator may be disclosed [*Strogatz*, 1994; *Abarbanel*, 1996; *Addison*, 1997].

2.3. Phase Space

[7] Even if chaotic systems are deterministic, meaning that their future dynamics are fully determined by their initial conditions, their evolution is not predictable. It is important to establish a vector space (called phase space) which is the space of all possible states of a physical system, each state corresponding to one unique point in the phase space. Then, it is possible to study the dynamics of the system by studying the dynamics of the corresponding phase space points [*Kantz and Schreiber*, 2004].

[8] Phase space reconstruction is a technique developed in analyzing nonlinear dynamic systems. The basic idea of phase space reconstruction is that evolution of any variable of a system depends on all the other interacting variables of the same system. Therefore, the information of these related variables is hidden within the evolution of the one that has been chosen to represent the system. The system output for a single variable thus reflects the effects of all the other (unknown) variables on the observable signal. In order to reconstruct an "equivalent" set of variables that describes the system, one needs only to investigate one of the variables by adopting a stepped or delayed series as a new coordinate for the phase space. By repeating the process, the "equivalent" phase space can be obtained [*Takens*, 1981]. The process is called "space delay embedding." In summary, the delayed coordinate embedding allows us to generate a phase space representation of the dynamical system from a single scalar time or space series. Thus, given the series of a single observable variable, it is possible to reconstruct a topologically equivalent portrait of the behavior of the original multidimensional set of variables that describe the system. The purpose of space delay embedding is to unfold the projection back to a multidimensional phase space that is representative of the original system. To expand a one-dimensional signal into an m-dimensional phase space, each observation in the original signal $X(i)$ has to be substituted with vector:

$$X(i) = x(i), x(i+\lambda), x(i+2\lambda), \ldots, x[i+(m-1)\lambda], \quad (1)$$

where i is the space (time) index, m is the embedding dimension and λ is a given delay.

2.4. Recurrence Plots

[9] Usually, a phase space does not have a dimension which allows it to be pictured. Higher-dimensional phase spaces can only be visualized by projection into the two- or three-dimensional subspaces. *Eckmann et al.* [1987] introduced a tool which enables us enables us to investigate the m-dimensional phase space through a two-dimensional representation of its recurrences (recurrence plot: a statistical plot that shows a pattern that reoccurs). Even if a chaotic system would not recur exactly to the initial state, it approaches the initial state arbitrarily close.

[10] In practice, if a series is represented by n data one can list them in column A in a spreadsheet:

$$A = a_1, a_2, a_3, a_4, a_5, \ldots, a_{n-3}, a_{n-2}, a_{n-1}, a_n. \quad (2)$$

[11] The same data may be also distributed in column to investigate the m-dimensional phase space through a two-dimensional representation of its recurrences. The recurrence plot allows us to extract

meaningful information from data on time and space series and reveals any redundancies inside the data. The same data may be also distributed in column B, delaying the series, e.g., for four steps ($\lambda = 4$, where λ is the delay step as defined in equation (1)):

$$B = a_{n-3}, a_{n-2}, a_{n-1}, a_n, a_1, \ldots, a_{n-7}, a_{n-6}, a_{n-5}, a_{n-4}. \quad (3)$$

[12] For n natural numbers and $\lambda = 4$, this arrangement corresponds to the couple of rows ordered as below:

$$A = 1 \quad 2 \quad 3 \quad 4 \quad 5 \quad 6 \quad 7 \ldots\ldots\ldots n-3 \quad n-2 \quad n-1 \quad n$$

$$B = n-3 \quad n-2 \quad n-1 \quad n \quad 1 \quad 2 \quad 3 \ldots\ldots\ldots n-7 \quad n-6 \quad n-5 \quad n-4$$

[13] The couples on the rows (a_1, a_{n-3}).....(a_n, a_{n-4}) represent a bidimensional projection ($m = 2$) of the phase space of the system that generates A (e.g., Figure 2). In the same way, the same set of values, distributed and stepped, in three columns (A, B, C):

$$A = a_1, a_2, a_3, a_4, a_5, \ldots, a_{n-3}, a_{n-2}, a_{n-1}, a_n, \quad (4)$$

$$B = a_{n-3}, a_{n-2}, a_{n-1}, a_n, a_1, \ldots, a_{n-7}, a_{n-6}, a_{n-5}, a_{n-4}, \quad (5)$$

$$C = a_{n-6}, a_{n-5}, a_{n-4}, a_{n-3}, a_{n-2}, \ldots, a_{n-9}, a_{n-8}, a_{n-7}, a_{n-6}, \quad (6)$$

generates a set of values on the rows (a_1, a_{n-3}, a_{n-7}) …(a_n, a_{n-4}, a_{n-8}), representing a three-dimensional projection ($m = 3$) of the same phase space.

[14] The goal of this reconstruction is to catch the states of the original system on the basis of the output values at the time (or position) of the observation (=sampling). In this way, each (unknown) state $S(i)$ is approximated by the vector of delayed coordinates (equation (1)):

$$X(i) = x(i), x(i+\lambda), x(i+2\lambda), \ldots, x[i+(m-1)\lambda].$$

Software S1 in the auxiliary material shows some examples of this procedure.[1]

[15] At any $S(i)$, a point P (defined by $X(i)$ in the phase space) moves on describing a trajectory (called phase space trajectory, or orbit). The evolution of the trajectory represents the dynamic of the system. One could expect that the evolution of the system with time tends to a dynamical stationary state, the subspace of which is the "attractor" of the dynamics. The set defined by all the points of delayed coordinates X is the attractor of the phase space. The "correlation" dimension (D) of the attractor [*Grassberger and Procaccia*, 1983] may be computed by evaluating the number $C(r)$ of pairs [X(i), X(j)], whose distance in the phase space is less than r:

$$|X(i) - X(j)| \leq r \; (j \neq i). \quad (7)$$

If

$$C(r) \propto r^D \quad (8)$$

exponent D is the correlation dimension of the attractor and a simple measure of the topological dimension of the attractor (Figure 3). Noteworthy, the dynamics is "chaotic" when the attractor is "strange," that is it represents an attracting set in the embedding phase space for which D has a fractional value. Trajectories along a strange attractor appear to skip around randomly but do not fill the whole phase space [*Strogatz*, 1994; *Abarbanel*, 1996; *Addison*, 1997]. It is possible to verify if an attractor is strange in the phase space by determining the correlation dimension D as a function of the embedding dimension m. Actually, a graphical visualization of the trajectory enables the determination of a state, since its shape gives hints about the system. Using logarithms, equation (8) can be written as:

$$\log[C(r)] = D \log(r) + q \quad (9)$$

where D is the slope of the linear regression of the graph log [(Cr)] versus log (r) and q is the intercept.

[16] Periodic or chaotic systems have characteristic phase space portraits. The space series is random and the attractor cannot be reconstructed when D increases with increasing m (Figure 3b). Otherwise, the space series is chaotic and the attractor is strange when D saturates to some fractal value $D_{\max}$ as m increases, above a critical value m_c [e.g., *Strogatz*, 1994; *Abarbanel*, 1996; *Addison*, 1997; *Poli and Perugini*, 2002] (Figures 3a and 3c).

2.5. Embedding Dimension m and Delay λ

[17] In general, if m is larger than twice the number of active degrees of freedom, regardless of how high the dimensionality of the reference space is, the attractor formed by $X(i)$ is equivalent to the original

[1] Auxiliary materials are available in the HTML. doi:10.1029/2009GC002798.

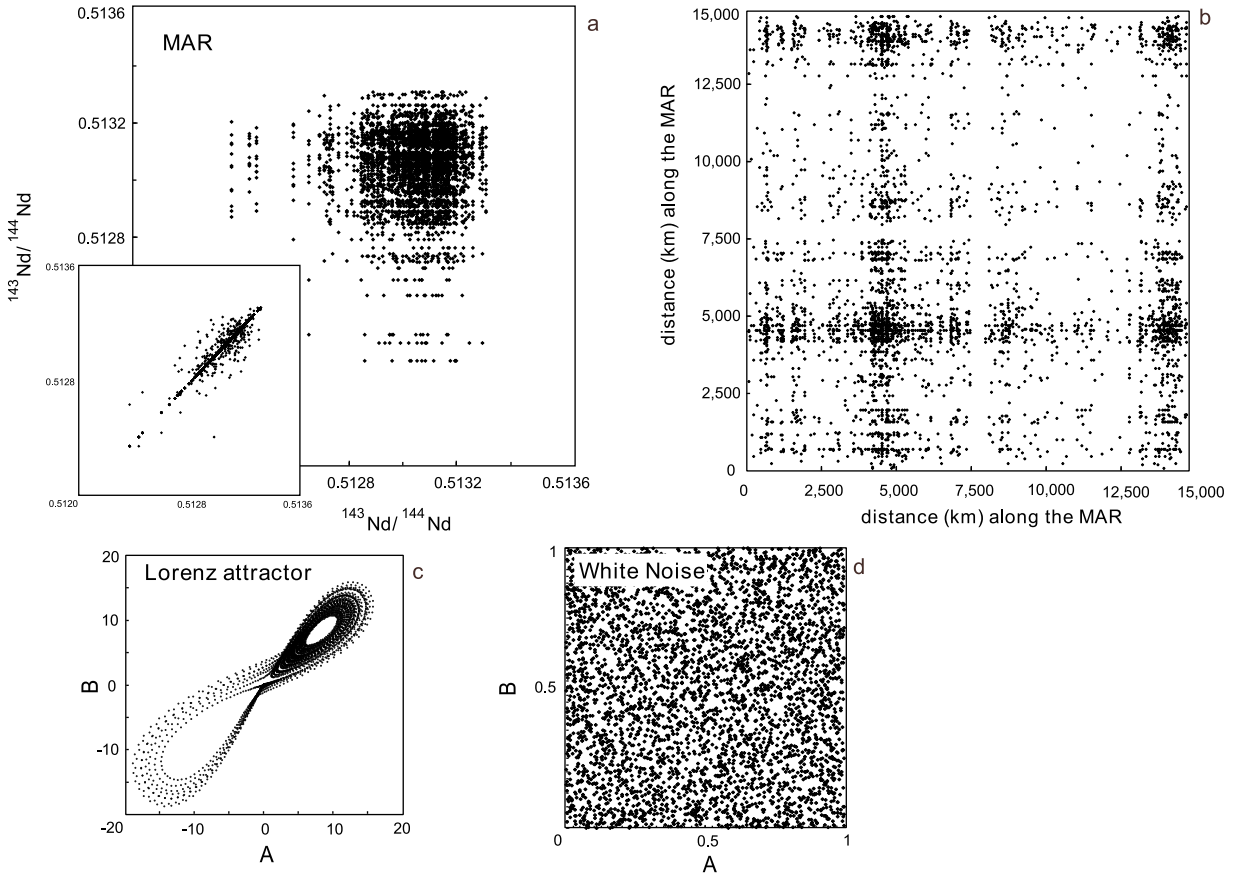

Figure 2. (a) Recurrence plots for Nd isotope series (MAR). Data are randomly arranged (irrespective of sampling location; some values are more recurrent than others and tend to cluster in a portion of the plot) and ordered with respect to increasing distances from the northernmost sample (inset in Figure 2a). According to *Tobler* [1970, p. 236], "Everything is related to everything else, but near things are more related than distant things" (spatial dependency in mathematical statistics); samples taken close together in general tend to be more similar in composition than samples taken farther apart. (b) Sample distances along the ridge treated as a space series and arranged with respect to increasing values of Nd isotope data, suggesting a kind of self organization in the data set with the "typical" value of about 5000 km. (c) The Lorenz series [*Lorenz*, 1963] and (d) the white noise. These plots represent a bidimensional projection ($m = 2$) of the phase space of the system, according to equation (3), and allow us to reveal the structure of the data set in the m-dimensional phase space through a two-dimensional representation of its recurrences. Note that the space series of Nd isotopic compositions for the MAR (Figure 2a) and the Lorenz series (Figure 2c) show an attractor in which data points are more dense (recur) in the top right corner of the chart, not filling up the entire bidimensional space (anisotropic signal). By contrast, random signals (Figure 2b) are characterized by uniform distribution of data points, filling up the entire two-dimensional space. Organization in signals increases with decreasing of the number of independent variables, thus depending upon the fractal dimension of the set under study (e.g., the Lorenz series shows neater trajectories due to its lower degrees of freedom than the Nd isotope series). Software S1 in the auxiliary material shows some examples of this procedure.

trajectory $x(i)$, that is in the unknown space which the original system is defined. A natural data set reveals its structure on a limited number of scales of observation. Stately differently, if one chooses a too large or too small ruler for making measurements, one misses to reveal the structure of the data set. Roughly speaking, it means that it is impossible to see waves in the sea if looking at the Earth from the Moon, neither if you take the point of view of plankton. Smaller m values satisfying $m > D_{max}$ can be sufficient. By contrast, the choice of a too large value of m for chaotic data will add redundancy and thus degrade the performance of many algorithms [*Kantz and Schreiber*, 2004].

[18] One neither knows the number of active degrees of freedom, which is formally necessary to compute m, nor having any idea of how to choose the delay λ, when starting to analyze a scalar time or space series. For ideal noise-free data, there exists a dimension m

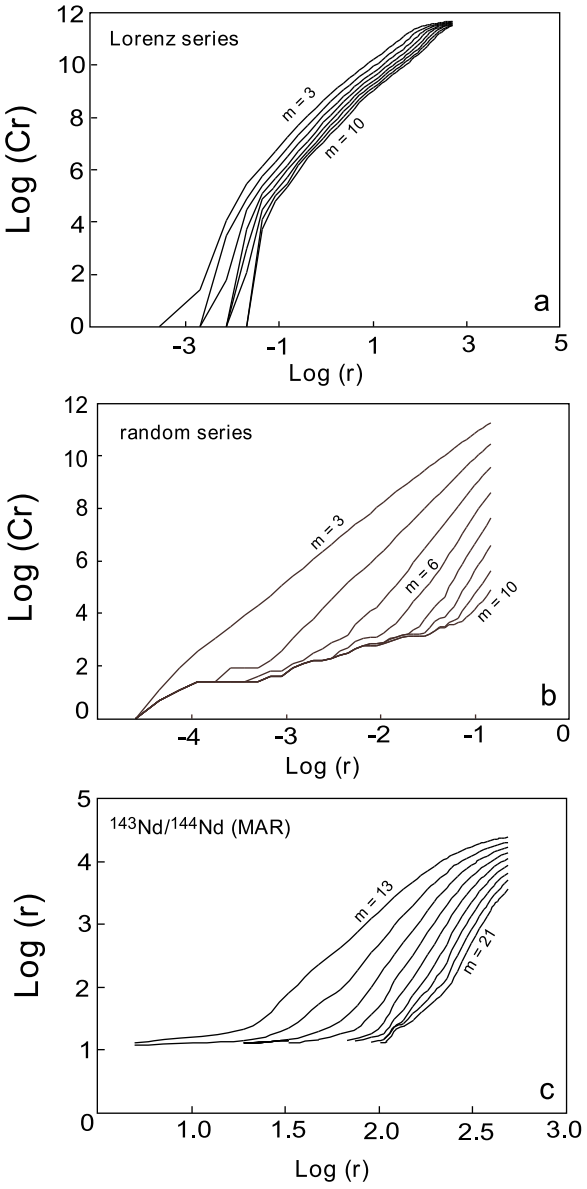

Figure 3. Log [$C(r)$] versus log (r) plots for (a) the Lorenz series (D_{max} = 2.06 and λ = 1), (b) a random (randomly generated) series ($D_{max} = \infty$), and (c) Nd isotope series (MAR; D_{max} = 5.1 and λ = 1). D is the slope of the linear regression of the graph log [(Cr)] versus Log (r), according to equation (11).

such that the vectors x(i) are equivalent to phase space vectors. Generally, there are two different approaches for optimizing the embedding parameters m and λ: either, one starts with the intended analysis right away and optimizes the result with respect to m and λ, that is by increasing the values of m until the typical behavior of deterministic data appears (e.g., chaos manifests itself); or one exploits specific statistical tools for their determination and uses the optimized values for further analysis [*Cao*, 1997; *Kantz and Schreiber*, 1997]. We used both the approaches to determine the correct values of m and λ.

2.6. Determination of *m* and False Near Neighbors

[19] The embedding dimension can be assessed by the smallest number of the uncorrelated directions in the phase space, that is the minimum number of delay coordinates needed so that the trajectories $x(i)$ do not intersect in m dimensions. This can be done by means of various methods which are based on the principle that, by decreasing the dimension, an increasing amount of phase space points will be projected in the neighborhood of any phase space point, even if they are not real neighbors. The method of finding a proper m can be described using geometrical considerations: as m increases, attractors "unfold" and the vectors that are close in dimension m move to a significant distance apart in (m + 1), being "false near neighbors" in dimension m. In dimensions less than m, trajectories can intersect because their projected down into too few dimensions. Subsequent calculations, such as predictions, may then be corrupted. If it is too large, noise and other contamination may corrupt other calculations because noise fills any dimension.

[20] The method of false near neighbors [*Kennel et al.*, 1992] measures the percentage of false neighbors as m increases. If we assume that the dynamics in phase space is represented by a smooth vector field, then neighboring states should be subject to almost the same evolution. Hence, after a short time interval into the future, the two trajectories emerging from them should be still close neighbors, even if chaos can introduce an exponential divergence of the two. A certain embedding dimension is sufficient for a reconstruction of a phase space thanks to this property. The basic ideas is to search for points in the data set which are neighbors in embedding space, but which should not be neighbors since their future temporal evolution is too different. Imagine that the correct m for some data set is m_0. Now study the same data in a lower-dimensional $m < m_0$. The transition from m to m_0 is a projection, eliminating certain axes from the coordinate system. Hence, points whose coordinates which are eliminated by the projection differ strongly, can become false neighbors in the m-dimensional space. For each point of the series, take its closest neighbor in m dimensions, and compute the ratio of the distances between these two points in m + 1 dimension and in m dimension. If this ratio is larger

than a given threshold, the neighbor was false. This threshold has to be large enough to allow for exponential divergence due to deterministic chaos [*Kantz and Schreiber*, 2004]. This situation has been discussed by *Armienti and Gasperini* [2007] for mantle isotopic composition and corresponds to the trivial observation that if two rock analyses have similar amounts of two elements A and B and, in a plot of A versus B they fall practically in the same position, nonetheless they may be completely different. Thus the dependence of the amount of these false nearest neighbors from m can be used to derive estimates of the embedding dimension in order to find the minimal one that is able to arrange all the points in distinct positions in the phase space [*Kantz and Schreiber*, 1997].

2.7. Determination of λ

[21] Analytical methods for estimating the delay λ are the autocorrelation and power spectrum functions, the average mutual information function (MIF), the degree of separation function, and the Lyapunov exponents [e.g., *Fraser and Swinney*, 1986]. The delay λ must be a large enough that independent information about the system is in each component of the vector. However, λ must not be so large that the components of the vectors x(i) are independent with respect to each other. Conversely, if the delay is too short, the vector components will be independent enough and will not contain any new information, then successive elements of the delay vectors are strongly correlated. We stress that λ has to be related to the average distance of the data point in the study series. In fact, stepping the sampling by λ implies to choose a value for spacing the samples of a mean value $\lambda \cdot F$, where F is the ratio between the temporal, or spatial extent, of the data series and the number of samples.

[22] A possible rule for good delay λ is to use the first minimum of the Average Mutual Information [*Fraser and Swinney*, 1986]. MIF is a measure of the dependence between two variables and determines how much information the measurements $x(i)$ at some time or space position have relative to measurements and some other time or space position $x\ (i + \lambda)$. If the two variables are independent, the mutual information between them is zero. If the two are strongly dependent, e.g., one is a function of another, the mutual information between them is large. There are other interpretations of the mutual information, for example, the stored information in one variable about another variable, and the degree of the predictability of the second variable by knowing the first. The delay λ should be chosen such that the elements in embedding vectors are no longer correlated, thus subsequent analysis would reveal spatial or geometrical structures. The optimal delay corresponds to the first minimum in the MIF and allows chaos to manifest itself [e.g., *Belaire-Franch and Contreras*, 2002; *Cellucci et al.*, 2005].

[23] The method used to reconstruct the attractor [*Takens*, 1981] and the algorithm employed to measure its topological dimension [*Grassberger and Procaccia*, 1983] would require data points to be evenly spaced. However, a constant sampling rate is not always possible in nature, and measurements result in discrete time (space) series which often lead to problems in applying standard methods of data analysis. Conversely, nonlinear data analysis allows an appropriate reconstruction of the underlying dynamics, since each single component of a system contains essential information about the dynamics of the whole system. We performed a numerical experiment on the Lorenz series (3500 data points; $D_{max} = 2.06$), by randomly extracting 3000, 2500, 2000,…., 500 data points that were treated as different time subseries, in order to evaluate enduring of the fractal dimension of the original series despite irregular sampling. For subseries made of number of points $\geq$1000 (thus about one third of the original samples of the Lorenz series), scale invariance is observed, with D_{max} ranging from 2.16 to 2.45, even if the signal has degraded by the increase of the average distance among the points. For time subseries made of number of points <1000, self-similarity cannot be proved, since the average distance of the elements in the series is too large to ensure the preservation of any relations between two subsequent points. In other words, a source may reveal its features provided that the average distance of the data points is small enough. Apparently, the error in evaluating the fractal dimension of a randomly sampled chaotic structure results in an overestimation of its correlation dimension D. A similar approach has been adopted by *Malinowski* [2004] leading to similar conclusions.

2.8. Application to Ocean Ridge Basalts

[24] We selected 1476 fresh basaltic samples from the Mid-Atlantic Ridge (from 78°N to 55°S (Figure 1)) and 519 from the East Pacific Rise (from 27°N to 56°S (Figure 1)), from the PetDB (http://www.petdb.org/) and GeoROC (http://georoc.mpch-mainz.gwdg.de/Start.asp) databases, and new high-quality data from *Agranier et al*. [2005]. By contrast,

database on the Indian Ridge consists of a number of analyses (about 250 (http://georoc.mpch-mainz.gwdg.de/Start.asp and *Meyzen et al*. [2007]) which is too small and patchy to be taken into account. We processed the raw available database by choosing only one isotopic datum for each coordinate and avoiding data on transform faults along the ridge. This choice is justified by the evidence that the difference in composition among samples from the same site is less than the variability of the nearest neighbors. Gaps in sampling exist for both the MAR and EPR, and in our modeling we took into account evidence that the database for the EPR is significantly more patchy (Figure 1). We parameterized the isotopic (Sr, Nd, Pb and Hf) heterogeneities of the asthenospheric mantle along the MAR and EPR as a function of their position along the ridge. We calculated the shortest distance between each two adjacent samples, then we assigned a position to each sample as the sum of the "orthodromic distances," starting from the northernmost sample (maximum latitude). The "orthodromic distance," or "great-circle distance," is the shortest distance between any two points on the surface of a sphere measured along a path on the surface of the sphere. Then, we determined whether the observed heterogeneity along each oceanic ridge could be described by a numerical model that is based on the theory of chaotic dynamical systems. We are aware that extracted data points are not evenly spaced along the orthodromic ridges, but the intrinsic structure of the geochemical heterogeneity of the upper mantle in these regions should manifest itself independently of the way of sampling, as discussed above for the Lorenz series.

[25] To recognize and characterize the dimension of the attractor related to isotope variability of the asthenosphere along the mid-ocean ridges, we assumed each sequence of isotopic compositions r_i and relative distance x_i from the northernmost sample as two different space series.

[26] We studied the structure of the data set, as sorted by distance (km) along the ocean ridges, by representing its phase space, and evaluating the fractal dimension of the correlation function that is obtained by counting the number of pairs of data whose Euclidean (E_d) distance in the phase space of dimension m is less than a given value r:

$$E_d = \sqrt{\sum_{m=0}^{m=M} (x(i+m\lambda) - x(i+k+m\lambda))^2} < r \qquad (10)$$

where i is the position, k a difference of positions between two points of the series, and λ is the delay as defined above, chosen as $\lambda = 1$ by computing the MIF. Let C_m the number of pairs which obeys equation (10).

[27] For $m = 1$ we take in consideration the space series itself, thus we have no need of delay and the Euclidean distance between two points is simply the difference in composition between two terms of the series, spaced of k:

$$|x(i) - x(i+k)| < r. \qquad (11)$$

A deeper insight of the data set is obtained by evaluating how many couples (X), within each different embedding dimension m, are found within a given segment of the ridge of a given length L. The rationale of this choice is a further theoretical development of nonlinear analysis. Consider two distances $L_m = m\lambda$ and $L_{m+1} = (m+1)\lambda$ along a ridge. Let C_m be the number of couples of measurements being spaced less than L_m and differing less than r, and $C_{(m+1)}$ the points at a distance less than $L_{m+1} = (m+1)i\lambda$ and differing less than r. If there is a relation of scale invariance between C_m and r ($C_m = K r^D$), it ensures that, varying m, the ratio C_m/C_{m+1} is provided by:

$$\frac{\mathrm{C}_{(\mathrm{m})}}{\mathrm{C}_{(m+1)}} = \frac{K_m r^D}{K_{m+1} r^D} = K. \qquad (12)$$

K is <1 when the number of pairs increases with the length of the segment in which we perform measurements, and K = 1 when $L \geq L_{\max}$, since the number of pairs necessarily stops increasing, when L is large enough to include all possible couples in the data set. In other words, C_{m+1} is larger than C_m only if L is smaller than a value ($L_{\max}$) behind which $C_{m+1} = C_m$, since all the points of the data set fulfill the condition to be at a distance $<L_{\max}$. Thus the meaning of $L_{\max}$ turns out promptly to be the maximum distance along the data series that still reveals the scale invariance relations.

[28] Plotting log [$C(r)$] ($C(r)$: the number of pairs of data whose Euclidean (E_d) distance in the phase space of dimension m is less than a given value r) versus log (r) (r: given value of compositional difference) in a bidimensional chart, the series is chaotic if the correlation dimension D, which is the slope of the curve for each m, saturates to $D_{\max}$ for a particular value m_c, that is (Figures 4a and 4c–4e)

$$D_{\max} = \text{constant, if } m \geq m_c. \qquad (13)$$

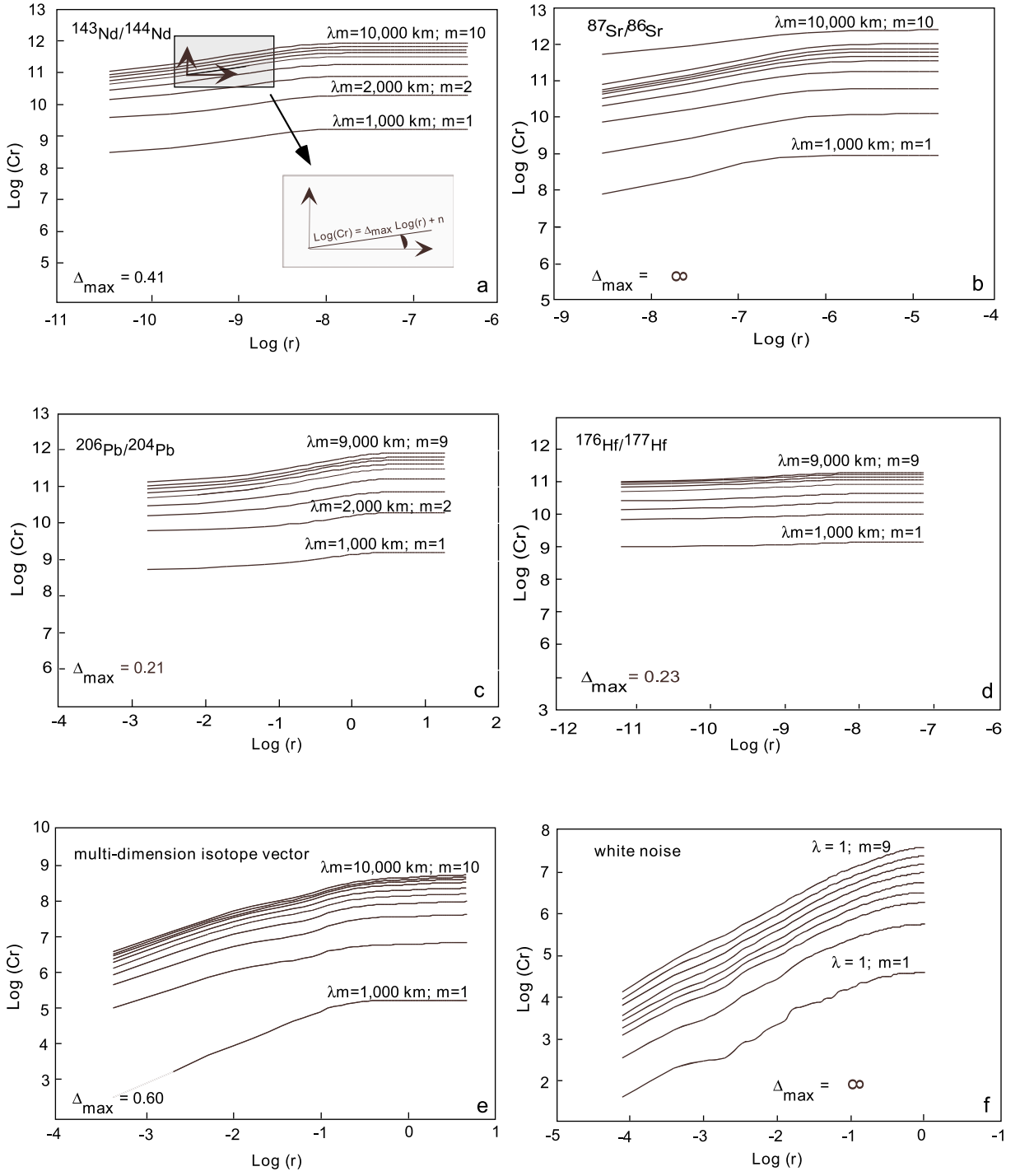

Figure 4. Plot of log [$C(r)$] versus log (r) for increasing values of the embedding dimension m (m = 1, 2, 3…, 10) for different space series along the MAR: (a) Nd isotopes, (b) Sr isotopes, (c) $^{206}Pb/^{204}Pb$ ratios, (d) Hf isotopes, (e) multidimensional isotope vector (λ = 1000), and (f) the white noise (λ = 1), here treated as a space series. Note that the attractor cannot be reconstructed when D increases with increasing m ($D_{max} = \infty$) such as for the Sr isotopes series and for the white noise (see section 2 for details). Software S2 in the auxiliary material contains the software adopted to apply the procedure to Nd data and provide plots and estimates of D.

Table 1. Characteristic Length Scales and Embedding Dimensions m of the Isotopic Variability of the Asthenosphere Along the MAR and EPR and D_{max} Values for Each Isotope Systematic and the Isotope Compositions as a Whole[a]

	Mid-Atlantic Ridge						Pacific Ocean					
Isotope Ratios	m	D_{max}	λ	L (km)	λ	Δ_{max}	m	D_{max}	λ	L (km)	λ	Δ_{max}
$^{87}Sr/^{86}Sr$	9	4.8	1	n.d.	1000	n.d.	9	4.5	1	6000	1000	0.48
$^{143}Nd/^{144}Nd$	8	5.1	1	5000	1000	0.41	8	4.9	1	6000	1000	0.36
$^{143}Nd/^{144}Nd$ (N)	8	4.6	1	5000	1000	0.35	n.c.	n.c.	1	n.c.	1000	n.c.
$^{143}Nd/^{144}Nd$ (S)	8	3.5	1	5000	1000	0.28	n.c.	n.c.	1	n.c.	1000	n.c.
$^{206}Pb/^{204}Pb$	7	4.1	1	6000	1000	0.21	7	4.2	1	6000	1000	0.39
$^{206}Pb/^{204}Pb$ (N)	7	4.0	1	5000	1000	0.32	n.c.	n.c.	1	n.c.	1000	n.c.
$^{206}Pb/^{204}Pb$ (S)	7	3.8	1	5000	1000	0.30	n.c.	n.c.	1	n.c.	1000	n.c.
$^{207}Pb/^{204}Pb$	7	6.0	1	6000	1000	0.18	n.c.	n.c.	1	7000	1000	0.25
$^{208}Pb/^{204}Pb$	7	4.2	1	5000	1000	0.20	n.c.	n.c.	1	7000	1000	0.32
$^{176}Hf/^{177}Hf$	n.c.	n.c.	1	5000	1000	0.23	n.c.	n.c.	1	n.c.	1000	n.c.
Σ(Sr, Pb, Nd, Hf)	n.c.	n.c.	1	5000	1000	0.60	n.c.	n.c.	1	5000 (no Hf)	1000	0.98

[a]Isotopes are Sr, Nd, Hf, Pb; see section 3 for details. Note that slightly higher length scales for the EPR might be due to more patchy database than for the MAR, nevertheless showing the same embedding dimension for the multidimensional vector. Abbreviations are as follows: n.c., not computed for scarce database; n.d., not determined, e.g., random (nonchaotic) distribution. We adopted a further constraint to explore the structure of the data set, by checking how a given distance along the ridge influences the estimate of m_c and D_{max}. By correlating $\log[C(r)]$ versus $\log(r)$ in bidimensional charts, L_{max} is the index referring to the characteristic distance (km) along the ridge for which the slope Δ reaches a maximum value of Δ_{Lmax}. $L = \lambda \cdot m$; errors on D_{max} and Δ_{max} are on the first and the second decimal digit, respectively.

Software S2 in the auxiliary material contains the software adopted to apply the procedure to Nd data and provide plots and estimates of D.

3. Results

[29] Once the space series for each isotope system and their relative cumulative distances are extracted, the existence of attractors in the system and whether their dimension is fractal can be evaluated by correlating log $[C(r)]$ versus log (r) in a bidimensional chart. By examining the behavior of D as m increases for both the MAR and EPR, we find the existence of chaotic behavior in most series (Table 1 and Figure 3). As a control we report the results of the numerical analysis we performed on the Lorenz series (Figure 3a) for which we obtain the value of D_{max} reported in the literature (D_{max} = 2.06 [*Abarbanel*, 1996]).

[30] For each isotope system, the space series of both the MAR and EPR are characterized by peculiar D_{max} values, ranging from 4.1 to 6.0 (Table 1). This variability might imply a peculiar sensitivity of the different isotopic systems in regard to processes responsible for the asthenosphere heterogeneity along the two mid-ocean ridges, since D_{max} corresponds to the number of degrees of freedom of the system under study.

[31] We adopted a further constraint to explore the structure of the data set by checking how a given distance L ($= \lambda \cdot m$) along the ridge influences the estimate of m_c and D_{max}. For different m_c we verified that the calculated values of the fractal dimension (here defined as Δ) is the same for each value of L along the ridge. Our value of λ, assessed at 1000 km by MIF, also corresponds to the ratio between the length of the orthodromic ridge and the number of points, scaled to a factor of 100 to avoid time consuming computation. We find that, for all the embedding dimensions, Δ reaches a maximum value (Δ_{max}) for $L \geq$ 5000–6000, depending upon the isotopic system under investigation (Figure 5). We interpret this result as revealing that the distribution of the asthenosphere heterogeneity along both the MAR and EPR is self-similar in the range of 5000–6000 km (Figures 4a–4d). Such a size for a mantle region is comparable for most of the isotope series, despite the different values of Δ_{max} (Figure 5).

[32] This result is supported by analysis of the large-scale structure (typology) and small-scale structure (texture) of the recurrence plots [*Eckmann et al.*, 1987; *Iwanski and Bradley*, 1998; *Choi et al.*, 1999], in which higher-dimensional phase spaces can be visualized by projection into the two (e.g., $^{143}Nd/^{144}Nd$ (Figure 2a)) or three-dimensional subspaces, for each isotope series. Actually, global impression from the typology is characterized by drift (trend) of points, likely caused by slowly varying parameters. If the data set is randomly arranged, the recurrence plots of isotope series show poorly populated top left and bottom right corners, induced by the scarcity of the association of couples of values typical of that region (e.g., Figure 2a). In this particular case, texture reveals vertical and horizontal lines, marking a space (isotope) length in

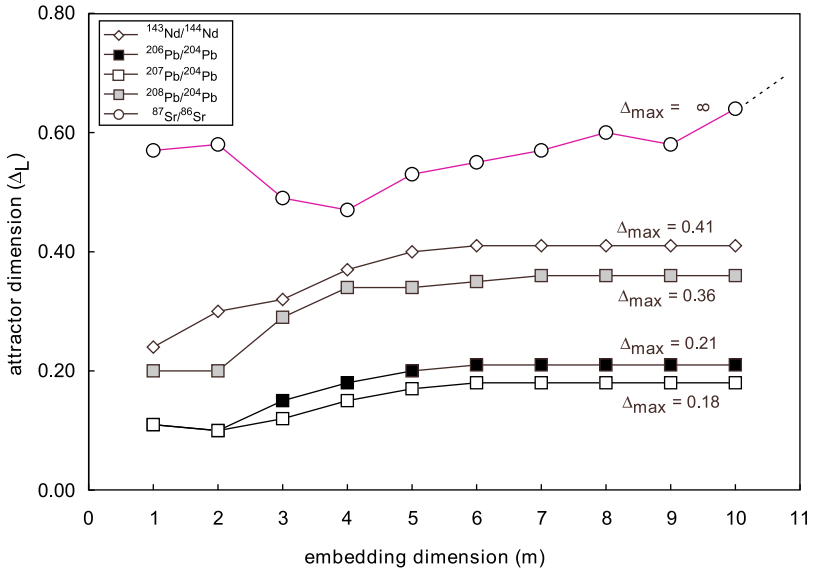

Figure 5. Variation of the fractal dimension of the attractor (Δ) versus the embedding dimension (m) for the space series extracted from the isotope compositions of the MAR. The attractor cannot be reconstructed when Δ_L increases with increasing m ($\Delta_{max} = \infty$) as for $^{87}Sr/^{86}Sr$ ratios. Conversely, Δ_L saturates to Δ_{max} for the space series extracted from the Nd and Pb (and Hf, not shown) isotope compositions.

which a state does not change or changes slowly, as if the corresponding region behaves coherently for some lapse of time (e.g., coherent mixing regions of *Perugini and Poli* [2000]). This is a typical behavior of laminar states [*Eckmann et al.*, 1987]. The occurrence of periodic patterns implies the occurrence of cycles in the underlying process: the distance between periodic patterns corresponds to the typical temporal or spatial step. A qualitative estimation of this period from Figure 2a is of about 0.0006 for the $^{143}Nd/^{144}Nd$ ratio in the MAR. Conversely, if the isotope series is ordered with respect to increasing distance from the northernmost sample along the ridges, in order to evaluate spatial relationships in the isotope geochemistry of the asthenosphere, the texture of the recurrence plots of isotope series reveal the presence of diagonal lines, which indicates that different trajectories visit the same region of the phase space at different times (inset in Figure 2a). Also this feature has been correlated to the development of chaotic behavior [*Eckmann et al.*, 1987]. Finally, the evidence that ordering with respect to the values of Nd isotopes produces a regular pattern in the distance recurrence plot suggests a kind of self organization in the data set with the "typical" value of abut 5000 km (Figure 2b).

[33] Distributions of both Nd and Pb isotope ratios of samples located along the MAR above (positive latitude) or below (negative latitude) the equator show slightly different D_{max}. Asthenosphere heterogeneity along the MAR in the southern hemisphere seems to reflect chaotic dynamics governed by a lower number of degrees of freedom with respect to the northern hemisphere (Table 1).

[34] We also defined the position of each sample in a six-dimensional space as a function of its Sr, Nd, Hf and Pb isotope compositions, generating a space series in which the elements are the Euclidean distance of each point from the others in the multidimensional space of isotope compositions. This allows us to avoid problems deriving from the occurrence of false nearest neighbors in the reconstruction of time series [e.g., *Kennel et al.*, 1992]. Also the distributions of such series show fractal features on the length scale of 5000 km for both the MAR and EPR (Figure 4e).

[35] In spite of the richness of isotopic data on MAR samples, which allows detailed analysis of the organization of isotopic composition of its underlying mantle, there are too few immobile trace element data to independently constrain the model from elemental point of view. However, we applied our analysis to data series provided by $^{207}Pb^*/^{206}Pb^*$ and $^{208}Pb^*/^{206}Pb^*$ [the ratio of the radiogenic additions to the initial terrestrial lead, defined as $[(^{208}Pb/^{204}Pb) - (^{208}Pb/^{204}Pb)_{init}]/[(^{206}Pb/^{204}Pb) - (^{206}Pb/^{204}Pb)_{init}]$ [*Hofmann*, 1997] that both represent a proxy of time integrated Th/U ratio, independently of elemental Pb. Results obtained from this analysis are similar to those for the other iso-

topic systematics. Since Th and U are immobile elements with respect to mantle mineralogy, we argue that the complexity that this approach reveals is likely related to the physical arrangement of mantle structure.

4. Discussion

[36] Fractals and scale-invariant structures are produced when, repeatedly, the output of a process represents the input for the following stage of the same process. The existence of strange attractors in the distribution of the isotopic composition of the asthenosphere sampled at ridge crests reveals the recurrence (or, more specifically termed, "recursion") of the same mantle process(es), endured over long periods of time. The spatial structure of the data set of the isotopic compositions of the ridge basalts is "self-similar" in the compositional interval defined by the embedding dimension *m*. Such interval is associated with a scale-invariant region reflecting maximum heterogeneity of the entire system. This implies that the length scale of 5000–6000 km in which self similarity develops, is the size in which all geochemical variability of the mantle source is wholly reflected, and beyond which one cannot find further peculiarities not yet observed. Such a typical dimension and compositional interval are not confined to a single ridge system nor to specific positions along the ridges: this strongly suggests the occurrence of some process characterizing the Earth's mantle on a planetary scale.

[37] In their pioneer paper, in spite of the limited number of data, *Zindler and Hart* [1986] proposed that maximum heterogeneity (amplitude ratio) of Sr, Nd and Pb isotope compositions for various volcanoes, ocean islands and ridge segments results at the length scale of 1000–10000 km.

[38] Actually, even isotopic compositions of the MAR and EPR are not homogeneous along the ridges and typical NMORB values are not widespread. Isotope patterns for both the ridges are characterized by spikes in $^{87}Sr/^{86}Sr$ and $^{206}Pb/^{204}Pb$ ratios and troughs in Nd and Hf isotope values at various locations, some of which apparently relate to plume-ridge interactions (e.g., Iceland, Azores, Easter, Galapagos). This rough evaluation of isotope heterogeneity in mid-ocean ridges leads one to assign a crucial role to deep mantle upwelling related to hot spots. Hot spots would be able to dramatically modify the geochemistry of mantle asthenosphere, at least at long wavelengths, thus somehow delimiting distinct convective domains. This tenet has been adopted in recent studies on isotope geochemistry [*Agranier et al.*, 2005; *Blichert-Toft et al.*, 2005; *Meyzen et al.*, 2007] and profiles of gravity and topography [e.g., *Goslin et al.*, 1998], showing very long wavelengths variation (~1000 and ~5000 km) along ridge crests.

[39] Conversely, *Lecroart et al.* [1997], working on major element composition of the MAR, showed that the contribution of plume melts does not correlate with the geoid, assessing that the role of hot spot material is marginal in contaminating ridge basalt geochemistry. *Anderson* [1998, 2006] reached similar conclusions from different arguments, suggesting that the length scale of mantle heterogeneity is not necessarily related to thermal and chemical pollution induced by hot spots. With the SUMA model, *Meibom and Anderson* [2004] assessed that the upper mantle, is a "marble cake" structure caused by recycling and other plate tectonic processes but not related to deep mantle plumes or stirring of the upper mantle by convection [*Allègre and Turcotte*, 1986]. Convection would be passive and strongly controlled by surface conditions (upper mantle) and the history of subduction [*Anderson*, 1998].

4.1. Length Scale of 5000–6000 km

[40] The dimension of order 5000–6000 km is recurrent in geodynamics, topography and tomography literature and relates to surface waves which exhibit a peak in their amplitude at wavelengths corresponding to $l = 5$ or 6 [*Nakanishi and Anderson*, 1984a, 1984b]. As exhaustively discussed by *Anderson* [1998], at $l = 6$ residual topography correlates with seismic velocities between 200 and 500 km depth [*Cazenave and Thoraval*, 1994] and to the spectral peak at spherical harmonic degree 6 of hot spots [*Kedar et al.*, 1993].

[41] Because long-wavelength geoid anomalies in isostatically compensated regions can be directly related to the local dipole moment of the density-depth distribution, continental topography are proportional to the elevation multiplied by the mean depth of compensation. Thus, for a particular elevation, the greater the average depth of the isostatic "root," the larger the geoid anomaly. Thick cratons have an $l = 6$ expansion that correlates with other geophysical observables and is almost exactly the same as the anti–hot spot pattern [*Kedar et al.*, 1993]. Even if lower mantle density variations might be responsible for the long-wavelength geoid, the dimension of 5000–6000 km could be an iso-

statically compensated near-surface effect of the distribution of continental cratonic roots (depth ~200 km [*Polet and Anderson*, 1995]; up to ~350 km [*Artemieva and Mooney*, 2002]) into the upper mantle [*Wen and Anderson*, 1997; *Anderson*, 1998]. It has been proposed that the spacing and location of thick Precambrian cratons may control the pattern of convection ($l = 6$) and heat loss in the upper mantle, thus ruling the location of upwellings [e.g., *Chapman and Pollack*, 1974; *Anderson*, 1998]. Actually, $l = 6$ spherical harmonic also represents a peak in upper mantle convective power in numerical simulations [e.g., *Tackley et al.*, 1994].

[42] Finally, a value of about $6–8 \cdot 10^6$ km^2 is also considered a critical dimension for the fate of cratons: since larger cratons have thicker (>300 km) keels, they would skip the effect of heat accumulation at depth. Conversely, smaller cratons would be less efficient in diverting the heat, hence more subject to erosion by mantle convection until an equilibrium lithospheric thickness of about 220 km is reached [*Artemieva and Mooney*, 2002]. Consequently, the reworking of Archean crust could have lead to the coexistence and evolution of two different main craton sizes, characterized by both peculiar average length (lower or higher than 6000–8000 km), and keel thickness (~220 km and >300 km, respectively).

[43] The dimension of 5000–6000 km we identified as a recurrent size for self-similar structures characterizing both the MAR and EPR is also indeed a significant dimension of the spectral peak at spherical harmonic degree 6 of hot spots, cratons and several other geophysical observables. These features do refer to the present distribution of lithospheric and asthenospheric elements and their geodynamics, but they could be inherited by the past history of our planet.

[44] In summary, $l = 6$ peak (6000 km corresponds to about 1/6 of the Earth circumference) seems to represent a characteristic length scale for the whole Earth: how it could be related to the length scale compositional self-similarity of ridge axes is intriguing.

4.2. Viable Mechanisms Inducing Compositional Scale Invariance

[45] The typical pace of about 6000 km of all quoted geophysical observables has a profound difference with respect to the length scale of compositional invariance we document for the asthenosphere sampled at ridge crests. In fact, while $l = 6$ implies some kind of physical discontinuity in present-day spatial distribution of the geophysical observables, the length scale of maximum variability of mantle isotopic composition is continuous in space (and time?), being independent of where a segment of 6000 km is placed along the ridge. This implies that the mechanism at the base of compositional scale invariance is intrinsic to the dynamics of the whole asthenosphere.

[46] At the state of the art, the mechanism which can play such a long-lasting and pervasive role in asthenosphere evolution is represented by the cyclic route of "partial melting, melt extraction and recycling" [*Meibom and Anderson*, 2004; *Rudge et al.*, 2005], in a "bottom to top," or "top to bottom," thermal or athermal driven mantle convection, which stretches and refolds lithospheric plates over geological time [*Agranier et al.*, 2005]. In this view, it is possible that 5000–6000 km may represent the largest length scale of mantle heterogeneity and could be related to the common size of the mantle regions which have been affected by the above mentioned cyclic route, favored by the mantle flow related to mantle stirring (athermal plate tectonics or thermal mantle convection). Such a route is a viable mechanism that could be able to induce scale invariance on a planetary scale, irrespective of the range of latitude of the ridge segments taken into account (Table 1). The dimension of the chaotic region could reflect the length scale of mantle chemical and fertility variations, that is related to the size of continental and oceanic plates. Migrating trenches and continents, and a mantle that is sampled by migrating ridges and thin spots, even in sluggish convective regime [*Korenaga*, 2006], can result in statistical compositional heterogeneity [*Anderson*, 2006]. Nevertheless, local mantle features appear to influence the chaotic structure of the upper mantle, perturbing its complexity but not its size. Actually, the southern hemisphere along the MAR, while showing self-similarity within the same size of 5000–6000 km as the northern one, is characterized by slightly lower D_{max} values, likely reflecting lower mantle anomaly, e.g., the Dupal anomaly. According to *Agranier et al.* [2005], this evidence could be interpreted as the effect of the northward convective dispersal ("reeling off") of the southern hemisphere anomalous mantle (Type B spectra in *Agranier et al.*'s [2005] periodograms).

[47] Nevertheless, it is fundamental that this behavior had been characterizing mantle dynamics for a significant number of cycles over the history of the Earth's upper mantle, before the asthenosphere acquired a chaotic structure. This condition requires

a large span of time and/or highly dynamic regimes, not observed in Phanerozoic plate tectonics. Phanerozoic crust is characterized by a large size range of continental and oceanic plates, and fast and slow spreading ridges coexist, as depicted by the present-day $l = 6$ peak. Moreover, given the present rate of lithosphere subduction, the maximum number of times that oceanic and continental plates might have been recycled in the mantle since the beginning of plate tectonics (about 2.7–3.1 Ga ago [*Condie and Pease*, 2008]; 1.8–2.0 Ga [*Stern*, 2007, 2008]) is relatively small (no more than 17, for average 180 Ma old oceanic floor [e.g., *Catalano et al.*, 2001]) and unlikely enough to induce scale invariance organization. Achievement of a chaotic structure needs a higher number of recursions of events in the same time span, rather suggesting highly dynamic behavior of the mantle, which would imply vigorous mantle convection, e.g., plume-like dynamics (high Rayleigh number: $R_a \geq 1.9 \times 10^5$).

4.3. From Fast to Sluggish Convection

[48] Thermal convection at infinite Prandtl number may relate low-order chaotic to high-order turbulent systems. At infinite Prandtl and high Rayleigh numbers ($R_a \geq 1.9 \times 10^5$), high-order truncations of the Saltzman equations [*Saltzman*, 1962]) yields chaotic solutions, suggesting that mantle convection may be a chaotic process, also in a regime of laminar fluxes [*Schubert et al.*, 2001; *Antonsen and Ott*, 1991]. The horizontal size of the convective cells are thought to be proportional to the size of the lithospheric plates [*Monnereau and Quéré*, 2001]. In this view, an asthenospheric region with a typical size of 5000–6000 km could be related to relatively large-size convective cells (on the order of thousands km). This condition is generally associated with weak (sluggish) mantle convection, a dynamical regime likely possible only after the Archean-Proterozoic boundary. During the Archean, mantle convection is commonly thought to have been more rapid and shallow ($R_a \geq 10^7$; "hard turbulence" [*Hansen et al.*, 1990, 1992; *van Thienen et al.*, 2004]), resulting in small convective cells and allowing only small, thin lithospheric plates, called microplates or microcontinents (on the order of hundreds km [e.g., *King*, 2005]). By the beginning of the Proterozoic, convection intensity decreased, since the mantle, ostensibly, underwent thermal changes that established much larger convection cells. This drove the formation of larger continental plates, as with the modern plate tectonics [e.g., *Breuer and Spohn*, 1995; *Peltonen et al.*, 2003; *Condie and Pease*, 2008].

[49] Plate size has increased through time, reflecting a peculiar organization of the convective regime which, we argue, is also recorded in the chaotic signature and typical size of mantle heterogeneities along the ridges. If the relationship "plate size – cell size – age" is correct, the typical length of the self-organized region along the ridges pin points a specific lapse of time in the Earth's history. The same size of the chaotic regions, characterizing wide mantle portions within the asthenosphere, would suggest a specific period in which 5000–6000 km was the general (widespread) magnitude of average plates. This may imply a surface arrangement characterized by tessellation of equidimensional plates [e.g., *Anderson*, 2002]. The common indicators of plate tectonics are weak before the Proterozoic, when high-temperature conditions allowed rapid subduction of young, hot slabs that could have melted before undergoing complete dehydration [*Abbott et al.*, 1994; *Taylor and McLennan*, 1995]. Different length scales of geochemical heterogeneity call for an upper mantle that had already underwent significant modification processes at the time of the onset of the recorded chaotic behavior (e.g., recycling of old, altered oceanic crust and mantle wedge metasomatism). This picture reflects a modern island arc regime more than a high-temperature/low-pressure subduction system as in the Archean. The size (~5000–6000 km) of the chaotic regions in the asthenosphere along the ridges would thus record a fundamental transition in the thermal conditions of the Earth's mantle, marking the shift toward a "sluggish convective" regime, which would have permitted the preservation of an early self organization of the upper mantle.

[50] In this view, geophysical features resulting in spherical harmonic wavelengths of $l = 6$ could be a remnant consequence, rather than the cause, of the observed mantle geochemical self organization on the length scale of 5000–6000 km.

5. Conclusions

[51] We propose a new method that allows us to detect the chaotic structure induced by convection and recorded by self organization of isotopic compositions along two of the main ridge axes (MAR and EPR). This relationship enables to identify the size (5000–6000 km) of mantle regions that lie beneath the ridges and show the entire compositional range of upper mantle isotopic variability. These regions should be considered as fossil remnants of mantle self organized structures related to an earlier convective regime. Our approach demonstrate the

occurrence of scale-invariant compositional heterogeneity in the asthenosphere mantle on the scale of 5000–6000 km, arguing that this is a result of convection mechanism.

[52] Actually, scale invariance calls for recursive processes, more easily acquired in high-dynamic convective regimes. At present, far away from plumes, mantle dynamics is in the regime of sluggish, possibly laminar flux but, in the past, thermal conditions could have allowed an extensive, more dynamic convective system [*Yuen et al.*, 1993]. The chaotic imprint in geochemical heterogeneity along the MAR and EPR mimics a marble cake mantle in which geochemical markers, reflecting processes of recycling, mixing, partial melting and metasomatism, coexist on decreasing length scale as indicators of mature plate tectonics [e.g., *Meibom and Anderson*, 2004; *Agranier et al.*, 2005]. The adopted method reveals the structure of the mantle, as it is sampled by MORB (= the structure of sampling), whatever is the compositional range of measurements. It means that we do not need to provide the entire range of isotope composition of MORB at MAR and EPR to prove that the arrangement of available data is chaotic. This implies that even if some composition of the MORB's zoo is missed by sampling, the structure of the sampled area is still well evident. Actually, according to our approach, it is possible that within the length scale of 5000–6000 there are MORB compositions not yet documented in the world wide repertory of MORB databases.

[53] We assess that the present-day distribution of chaotic mantle heterogeneity is frozen since the Proterozoic. The present-day sluggish convection regime still reveals its inherited structure on account of insufficient number of cycles completed since the convection regime has changed.

[54] In this view, we consider the length scale of 5000–6000 km as the maximum size of self organization in the upper mantle at the debut of the Proterozoic that still controls the large-scale spatial distribution of lithospheric features, e.g., cratons, hot spots, and geoid undulations of order 6.

[55] A further step requires the assessment of the vertical distribution of mantle heterogeneity, a task that we started to accomplish both thorough evaluation of spatial-temporal distribution of ocean floor tholeiite isotopic composition, and the study of volcanoes which have erupted lava series, sampling a suitable interval of mantle depths. This will lead to depict, at a given time, the position of mantle compositional domains in vertical regions.

Acknowledgments

[56] We are grateful to K. Putirka, M. Menzies, E. Mori, and M. Wilson for helpful discussion on the subject of this work. Comments by A. Meibom, A. Stracke, and an anonymous reviewer were immensely useful. Financial support was provided by MIUR (2005–2007, protocol 2005055415_002; G. Poli, "Dinamiche caotiche e geometrie frattali nella genesi e nel mescolamento dei magmi") and the Consolidated Research Groups (2005SGR-0795PEGEFA and 2009SGR-0972PEGEFA), funded by AGAUR-DURSI, Catalonian government.

References

Abarbanel, H. D. I. (1996), *Analysis of Observed Chaotic Data*, Springer, New York.

Abbott, D., L. Burgess, J. Longhi, and W. H. F. Smith (1994), An empirical thermal history of the Earth's upper mantle, *J. Geophys. Res.*, *99*, 13,835–13,850, doi:10.1029/94JB00112.

Addison, P. S. (1997), *Fractals and Chaos: An Illustrated Course*, Inst. of Phys., Bristol, U. K.

Agranier, A., J. Blichert-Toft, D. Graham, V. Debaille, P. Schiano, and F. Albarède (2005), The spectra of isotopic heterogeneities along the mid-Atlantic Ridge, *Earth Planet. Sci. Lett.*, *238*, 96–109, doi:10.1016/j.epsl.2005.07.011.

Allègre, C. J., and D. L. Turcotte (1986), Implications of a two-components marble-cake mantle, *Nature*, *323*, 123–127, doi:10.1038/323123a0.

Anderson, D. L. (1998), The scales of mantle convection, *Tectonophysics*, *284*, 1–17, doi:10.1016/S0040-1951(97)00169-8.

Anderson, D. L. (2002), How many plates?, *Geology*, *30*, 411–414, doi:10.1130/0091-7613(2002)030<0411:HMP>2.0.CO;2.

Anderson, D. L. (2006), Speculations on the nature and cause of mantle heterogeneity, *Tectonophysics*, *416*, 7–22, doi:10.1016/j.tecto.2005.07.011.

Antonsen, T. M., and E. Ott (1991), Multifractal power spectra of passive scalar convected by chaotic fluid flows, *Phys. Rev. A*, *44*, 851–857, doi:10.1103/PhysRevA.44.851.

Armienti, P., and D. Gasperini (2007), Do we really need mantle components to define mantle composition?, *J. Petrol.*, *48*, 693–709, doi:10.1093/petrology/egl078.

Artemieva, I. M., and V. D. Mooney (2002), On the relation between cratonic lithosphere thickness, plate motions, and basal drag, *Tectonophysics*, *358*, 211–231, doi:10.1016/S0040-1951(02)00425-0.

Belaire-Franch, J., and D. Contreras (2002), Recurrence plots in nonlinear time series analysis: Free software, *J. Comput. Graph. Statist.*, *11*, 996–997, doi:10.1198/106186002321018902.

Blichert-Toft, J., A. Agranier, M. Andres, R. Kingsley, J.-G. Schilling, and F. Albarède (2005), Geochemical segmentation of the Mid-Atlantic Ridge north of Iceland and ridge–hot spot interaction in the North Atlantic, *Geochem. Geophys. Geosyst.*, *6*, Q01E19, doi:10.1029/2004GC000788.

Breuer, D., and T. Spohn (1995), Possible flush instability in mantle convection at the Archean-Proterozoic transition, *Nature*, *378*, 608–610, doi:10.1038/378608a0.

Butler, R., J. M. Sinton, J. J. Mahoney, and S. M. Smaglik (1993), Spectral analysis of volcanic glass chemistry along the East Pacific Rise, 13°–23°S, *J. Geophys. Res.*, *98*(B7), 11,851–11,864, doi:10.1029/93JB00352.

Cao, L. (1997), Practical method for determining the minimum embedding dimension of a scalar time series, *Physica D*, *110*, 43–50, doi:10.1016/S0167-2789(97)00118-8.

Catalano, R., C. Doglioni, and S. Merlini (2001), On the Mesozoic Ionian basin, *Geophys. J. Int.*, *144*, 49–64, doi:10.1046/j.0956-540X.2000.01287.x.

Cazenave, A., and C. Thoraval (1994), Mantle dynamics constrained by degree-6 surface-topography, seismic tomography and geoid: Inference on the origin of the South Pacific superswell, *Earth Planet. Sci. Lett.*, *122*, 207–219, doi:10.1016/0012-821X(94)90061-2.

Cazenave, A., S. Houry, B. Lago, and K. Dominh (1992), Geosat-derived geoid anomalies at medium wavelength, *J. Geophys. Res.*, *97*, 7081–7096, doi:10.1029/91JB03127.

Cellucci, C. J., A. M. Albano, and P. E. Rapp (2005), Statistical validation of mutual information calculations: Comparison of alternative numerical algorithms, *Phys. Rev. E*, *71*, 066208, doi:10.1103/PhysRevE.71.066208.

Chapman, D. S., and H. N. Pollack (1974), Cold spot in West Africa: Anchoring the African plate, *Nature*, *250*, 477–478, doi:10.1038/250477a0.

Choi, J. M., B. H. Bae, and S. Y. Kim (1999), Divergence in perpendicular recurrence plots; Quantification of dynamical divergence from short chaotic time series, *Phys. Lett. A*, *263*, 299–306, doi:10.1016/S0375-9601(99)00751-3.

Condie, K. C., and V. Pease (2008), *When Did Plate Tectonics Begin on Planet Earth?*, *Spec. Pap. Geol. Soc. Am.*, *440*, 294 pp.

Debaille, V., J. Blichert-Toft, A. Agranier, R. Doucelance, P. Schiano, and F. Albarède (2006), Geochemical component relationships in MORB from the Mid-Atlantic Ridge, 22–35°N, *Earth Planet. Sci. Lett.*, *241*, 844–862, doi:10.1016/j.epsl.2005.11.004.

Eckmann, J.-P., S. O. Kamphorst, and D. Ruelle (1987), Recurrence plots of dynamical systems, *Europhys. Lett.*, *4*, 973–977, doi:10.1209/0295-5075/4/9/004.

Fraser, A. M., and H. L. Swinney (1986), Independent coordinates from strange attractors from mutual information, *Phys. Rev. A*, *33*, 1134–1140, doi:10.1103/PhysRevA.33.1134.

Goslin, J., J.-L. Thirot, O. Noël, and J. Francheteau (1998), Slow-ridge/hotspot interaction from global gravity, seismic tomography and $^{87}Sr/^{86}Sr$ isotope data, *Geophys. J. Int.*, *135*, 700–717, doi:10.1046/j.1365-246X.1998.00609.x.

Graham, D. V., J. E. Lupton, F. J. Spera, and D. M. Christie (2001), Upper-mantle dynamics revealed by helium isotope variations along the southeast Indian Ridge, *Nature*, *409*, 701–703, doi:10.1038/35055529.

Grassberger, P., and I. Procaccia (1983), Measuring the strangeness of strange attractors, *Physica D*, *9*, 189–208, doi:10.1016/0167-2789(83)90298-1.

Hansen, U., D. A. Yuen, and S. E. Kroening (1990), Transition to hard turbulence in thermal convection at infinite Prandtl number, *Phys. Fluids A*, *2*, 2157–2163, doi:10.1063/1.857802.

Hansen, U., D. A. Yuen, and S. E. Kroening (1992), Mass and heat transport in strongly time-dependent thermal convection at infinite Prandtl number, *Geophys. Astrophys. Fluid Dyn.*, *63*, 67–89, doi:10.1080/03091929208228278.

Hofmann, A. W. (1997), Mantle geochemistry: The message from oceanic volcanism, *Nature*, *385*, 219–229, doi:10.1038/385219a0.

Humler, E., J. L. Thirot, and J. P. Montagner (1993), Global correlations of mid-ocean-ridge basalt chemistry with seismic tomographic images, *Nature*, *364*, 225–228, doi:10.1038/364225a0.

Iwanski, J. S., and E. Bradley (1998), Recurrence plots of experimental data: To embed or not to embed?, *Chaos*, *8*, 861–871, doi:10.1063/1.166372.

Kantz, H., and T. Schreiber (1997), *Nonlinear Time Series Analysis*, 350 pp., Cambridge Univ. Press, Cambridge, U. K.

Kantz, H., and T. Schreiber (2004), *Nonlinear Time Series Analysis*, 2nd ed., 369 pp., Cambridge Univ. Press, Cambridge, U. K.

Kedar, S., D. L. Anderson, and D. J. Stevenson (1993), Relationship between hot spots and mantle structures: Correlation with whole mantle seismic tomography, in *Flow and Creep in the Solar System: Observations, Modelling and Theory*, edited by D. B. Stone and S. K. Runcorn, pp. 249–259, Kluwer, Dordrecht, Netherlands.

Kellogg, J. B., S. B. Jacobsen, and R. J. O'Connell (2002), Modeling the distribution of isotopic ratios in geochemical reservoirs, *Earth Planet. Sci. Lett.*, *204*, 183–202, doi:10.1016/S0012-821X(02)00981-0.

Kennel, M. B., R. Brown, and H. D. I. Abarbanel (1992), Determining embedding dimension for phase-space reconstruction using a geometrical construction, *Phys. Rev. A*, *45*(6), 3403–3411, doi:10.1103/PhysRevA.45.3403.

King, S. D. (2005), Archean cratons and mantle dynamics, *Earth Planet. Sci. Lett.*, *234*, 1–14, doi:10.1016/j.epsl.2005.03.007.

Klein, E. M., and C. H. Langmuir (1987), Global correlations of ocean ridge basalts chemistry with axial depth and crustal thickness, *J. Geophys. Res.*, *92*, 8089–8115, doi:10.1029/JB092iB08p08089.

Korenaga, J. (2006), Archean geodynamics and the thermal evolution of Earth, in *Archean Geodynamics and Environments*, *Geophys. Monogr. Ser.*, vol. 164, edited by K. Benn, J.-C. Mareschal, and K. C. Condie, pp. 7–32, AGU, Washington, D. C.

Lecroart, P., F. Albarède, and A. Cazenave (1997), Correlations of mid-ocean ridge basalt chemistry with the geoid, *Earth Planet. Sci. Lett.*, *153*, 37–55, doi:10.1016/S0012-821X(97)00140-4.

Lorenz, E. N. (1963), Deterministic non-periodic flow, *J. Atmos. Sci.*, *20*, 130–141, doi:10.1175/1520-0469(1963)020<0130:DNF>2.0.CO;2.

Malinowski, M. (2004), Hotspots and mantle plumes: Constraints from statistical analysis, *Acta Geophys.*, *52*, 337–348.

Mandelbrot, B. (1982), *The Fractal Geometry of Nature*, W. H. Freeman, New York.

Meibom, A., and D. L. Anderson (2004), The statistical upper mantle assemblage, *Earth Planet. Sci. Lett.*, *217*, 123–139, doi:10.1016/S0012-821X(03)00573-9.

Meyzen, C., J. Blichert-Toft, J. N. Ludden, E. Humler, C. Mével, and F. Albarède (2007), Isotopic portrayal of the Earth's upper mantle flow field, *Nature*, *447*, 1069–1074, doi:10.1038/nature05920.

Monnereau, M., and S. Quéré (2001), Spherical shell models of mantle convection with tectonic plate, *Earth Planet. Sci. Lett.*, *184*, 575–587, doi:10.1016/S0012-821X(00)00334-4.

Moore, J. C., S. Akber-Knutson, J. Konter, J. Kellogg, S. Hart, L. H. Kellogg, and B. Romanowicz (2004), Scales of mantle heterogeneity, *Eos Trans. AGU*, *85*(47), Fall Meet. Suppl., Abstract U41A-0715.

Nakanishi, I., and D. L. Anderson (1984a), Measurements of mantle wave velocities and inversion of lateral heterogeneity and anisotropy—II. Analysis by the single-station method, *Geophys. J. R. Astron. Soc.*, *78*, 573–617.

Nakanishi, I., and D. L. Anderson (1984b), Aspherical heterogeneity of the mantle from phase velocities of mantle waves, *Nature*, *307*, 117–121, doi:10.1038/307117a0.

Peltonen, P., I. Mänttäri, H. Huhma, and A. Kontinen (2003), Archean zircons from the mantle: The Jormua ophiolite revisited, *Geology*, *31*, 645–648, doi:10.1130/0091-7613(2003)031<0645:AZFTMT>2.0.CO;2.

Perugini, D., and G. Poli (2000), Chaotic dynamics and fractals in magmatic interaction processes: A different approach to the interpretation of mafic microgranular enclaves, *Earth Planet. Sci. Lett.*, *175*, 93–103, doi:10.1016/S0012-821X(99)00282-4.

Phipps Morgan, J., and W. J. Morgan (1999), Two-stage melting and the geochemical evolution of the mantle: A recipe for mantle plum-pudding, *Earth Planet. Sci. Lett.*, *170*, 215–239, doi:10.1016/S0012-821X(99)00114-4.

Polet, J., and D. L. Anderson (1995), Depth extent of cratons as inferred from tomographic studies, *Geology*, *23*, 205–208, doi:10.1130/0091-7613(1995)023<0205:DEOCAI>2.3.CO;2.

Poli, G., and D. Perugini (2002), Strange attractors in magmas: Evidence from lava flows, *Lithos*, *65*, 287–297, doi:10.1016/S0024-4937(02)00196-2.

Rudge, J. F., D. McKenzie, and P. H. Haynes (2005), A theoretical approach to understanding the isotopic heterogeneity of mid-ocean ridge basalt, *Geochim. Cosmochim. Acta*, *69*, 3873–3887, doi:10.1016/j.gca.2005.03.004.

Saal, A. E., S. R. Hart, N. Shimizu, E. H. Hauri, and G. D. Layne (1998), Pb isotopic variability in melt inclusions from oceanic island basalts, Polynesia, *Science*, *282*, 1481–1484, doi:10.1126/science.282.5393.1481.

Saltzman, B. (1962), Finite amplitude free convection as an initial value problem, *J. Atmos. Sci.*, *19*, 329–341, doi:10.1175/1520-0469(1962)019<0329:FAFCAA>2.0.CO;2.

Schubert, G., D. L. Turcotte, and P. Olson (2001), *Mantle Convection in the Earth and Planets*, 940 pp., Cambridge Univ. Press, Cambridge, U. K.

Stern, R. J. (2007), When and how did plate tectonics begin? Theoretical and empirical considerations, *Chin. Sci. Bull.*, *52*, 578–591, doi:10.1007/s11434-007-0073-8.

Stern, R. J. (2008), Modern style plate tectonics began in Neoproterozoic time: An alternate interpretation of Earth dynamics and history, When and how did plate tectonics begin on planet Earth?, *Spec. Pap. Geol. Soc. Am.*, *440*, 265–280.

Strogatz, S. H. (1994), *Nonlinear Dynamics and Chaos*, Addison Wesley, Reading, Mass.

Tackley, P. J., D. J. Stevenson, G. A. Glatzmaier, and G. Schubert (1994), Effects of multiple phase transitions in a three-dimensional spherical model of convection in the Earth's mantle, *J. Geophys. Res.*, *99*, 15,877–15,901.

Takens, F. (1981), Detecting Strange Attractors in Turbulence, in *Dynamical Systems and Turbulence*, *Lect. Notes in Math.*, vol. 898, pp. 366–381, Springer, Berlin.

Taylor, S. R., and S. M. McLennan (1995), The geochemical evolution of the continental crust, *Rev. Geophys.*, *33*, 241–265, doi:10.1029/95RG00262.

Tobler, W. (1970), A computer movie simulating urban growth in the Detroit region, *Econ. Geogr.*, *46*(2), 234–240, doi:10.2307/143141.

van Thienen, P., A. P. van den Berg, and N. J. Vlaar (2004), Production and recycling of oceanic crust in the early Earth, *Tectonophysics*, *386*, 41–65, doi:10.1016/j.tecto.2004.04.027.

Wen, L., and D. L. Anderson (1997), Slabs, hot spots, cratons and mantle convection revealed from residual seismic tomography in the upper mantle, *Phys. Earth Planet. Inter.*, *99*, 131–143, doi:10.1016/S0031-9201(96)03162-7.

Wessel, P., D. Bercovici, and L. W. Kroenke (1994), The possible reflection of mantle discontinuities in Pacific geoid and bathymetry, *Geophys. Res. Lett.*, *21*, 1943–1946, doi:10.1029/94GL01815.

Wessel, P., L. W. Kroenke, and D. Bercovici (1996), Pacific Plate motion and undulations in geoid and bathymetry, *Earth Planet. Sci. Lett.*, *140*, 53–66, doi:10.1016/0012-821X(96)00037-4.

Yuen, D. A., D. M. Reuteler, W. Zhao, A. P. Vincent, and A. V. Malevsky (1993), Hard turbulent thermal convection and thermal evolution of the mantle, *J. Geophys. Res.*, *98*, 5355–5373, doi:10.1029/92JE02725.

Zhang, Y., T. Tanimoto, and E. M. Stolper (1994), S-wave velocity, basalt chemistry and bathymetry along the Mid-Atlantic Ridge, *Phys. Earth Planet. Inter.*, *84*, 79–93, doi:10.1016/0031-9201(94)90035-3.

Zindler, A., and S. R. Hart (1986), Chemical geodynamics, *Annu. Rev. Earth Planet. Sci.*, *14*, 493–571, doi:10.1146/annurev.ea.14.050186.002425.